Resilience Assessment in Electric Power Systems Against Volcanic Ash

M. Saltos-Rodríguez[1], *Student Member, IEEE,* M. Aguirre-Velasco[1], *Student Member, IEEE*,
A. Velásquez-Lozano[1], *Student Member, IEEE*, D. Ortiz-Villalba[1], *Member, IEEE*
A. Villamarín-Jácome[2], *Graduate Student Member, IEEE*, and J.R. Haro[2]
[1]Universidad de las Fuerzas Armadas ESPE, [2]Universidad de Chile
[1]Sangolquí-Ecuador, [2]Santiago-Chile
[1][masaltos2, mxaguirre1, amvelasquez1, ddortiz5]@espe.edu.ec
[2][avillama, jharo]@ing.uchile.cl

***Abstract*—Electric power systems (EPS) are facing challenges worldwide due to the increased occurrence of high-impact, low-probability (HILP) events, such as natural hazards. In this context, the concept of resilience has been considered in several studies. However, few studies have addressed the assessment of EPS resilience against volcanic eruptions with a focus on electrical structure damage. This paper proposes a methodology to assess the impact of ash deposits on the EPS. The methodology uses data sampling from historical ash deposit events to obtain probability density functions to then apply a Monte Carlo simulation (MCS) that can characterize the event and assess its impact on the electrical infrastructure through vulnerability curves. In addition, a DC optimal power flow model (DC-OPF) under contingencies was implemented to quantify different resilience metrics in terms of energy supply capacity, operation, and the infrastructure of the power system. The proposed methodology was applied to the Ecuadorian National Interconnected System (NIS) to assess the impact of an eruption of the Cotopaxi volcano. The results show our methodological framework evaluates resilience in terms of operation and infrastructure in EPS against the ash deposit, allowing mitigation plans to be better formulated.**

***Index Terms*—Resilience metrics, volcanic eruption, ash deposit, Monte Carlo simulation.**

NOMENCLATURE

A. Sets

G	Set of thermal power plants
H	Set of hydropower plants
L, N	Set of transmission lines and buses
R	Set of solar and wind power plants
S	Set of contingency scenarios, includes scenario in normal state s=0

B. Parameters

$A_{i,s}$	Binary matrix of states of power plants by contingency scenario [0,1]
$A_{l,s}$	Binary matrix of transmission line states by contingency scenario [0,1]
$A_{n,s}$	Binary matrix of load/demand states by contingency scenario [0,1]
D_n	Peak load on each bus [MW]
F_l^{max}	Maximum capacity of transmission lines [MW]
fp_h	Plant factor of hydropower plants [p.u]
$fr(l)$	Sending or origin node of line l
$G_{i,s}$	Generation capacity connected
M	Big M, sufficiently large positive value
Ns	Number of Scenarios
$\overline{P_i^{max}}$	Installed capacity of the system's largest power plants "i" [MW]
P_i^{max}	Maximum power of power plants [MW]
$T_{l,s}$	Transmission lines in service
$to(l)$	Receiving or destination node of line l
x_l	Reactance of transmission lines [p.u]
α_r	Normalized factor of the natural resource available from solar and wind power plants [p.u]
γ	Percentage of the system's demand [p.u]
π_g^{op}	Operating cost of thermal power plants [$/MWh]

C. Variables

$ENS_{n,s}$	Energy Not Supplied in each bus by contingency scenario [MWh]
$f_{l,s}$	Power flow through transmission lines in each contingency scenario [MW]
P_i	Power generated from power plants by contingency scenario [MW]
$R_{i,s=0}^{up}$	Up-turn reserve of power plants, excludes solar and wind power plants [MW]
$\delta_{n,s}$	Voltage angle on each bus and contingency scenarios [rad]

I. INTRODUCTION

Electric power systems (EPS) are critical for the development and survival of modern societies; unfortunately, those systems face challenges worldwide due to the increased occurrence of high-impact, low probability (HILP) events, such as natural hazards. These events produce significant economic and social losses due to structural damage in the electrical supply infrastructure, resulting in the loss of critical services for an extended time. The traditional reliability analysis framework in which these systems have been designed, built, and operated is generally insufficient to deal with HILP events. Therefore, the concept of resilience has been considered in several studies that propose strategies to deal with possible natural hazards [1], [2]. However, only a few studies have addressed the assessment of resilience in electrical networks against volcanic eruptions [3]–[5].

Volcanic eruptions rank as one of the most devastating events worldwide since their occurrence is linked to the partial or complete destruction of multiple population centers and

2022 IEEE Power & Energy Society General Meeting (PESGM) | 978-1-6654-0823-3/22/$31.00 ©2022 IEEE | DOI: 10.1109/PESGM48719.2022.9916989

their incidence can affect the infrastructure of EPS. Among the agents derived from a volcanic eruption, ash deposit is what most commonly causes structural damage to the components of a power system [6]. For instance, in May 2008, the eruption of the Chaitén volcano caused the shutdown of the Futaleufú hydroelectric plant in Argentina. This shutdown resulted from ash deposit causing flashovers in the circuit breaker columns of the hydroelectric control station and explosions in the high voltage insulators of the 240 kV transmission lines adjacent to the station [7]. Likewise, in 2011 after the Cordón Caulle volcano erupted there were continuous power outages (with 40% of the town without power) in the city of Villa La Angostura, Chile because ash deposits caused failures in a power plant, the transformation centers, and the insulation of transmission lines [8]. The electrical infrastructure damage associated with ash deposits has been recorded and studied worldwide [9], [10]. These studies confirm that ash deposits cause prolonged blackouts, loss of electrical components, and socio-economic losses due to the paralysis of strategic sectors, such as the health, food industry, transportation, and others.

Given the scale of the problem described above, this paper proposes a novel methodology to assess the resilience of the EPS against volcanic hazards, focusing on the effects of ash deposits. The main contributions of this paper are described as follows: i) A volcanic ash deposit model and impact assessment on the EPS: the proposed methodology includes a data sampling of historical ash deposit events to obtain probability density functions with which to perform Monte Carlo simulations (MCS) to characterize a volcanic event and assess its impact on the EPS infrastructure through vulnerability curves. ii) Real-World case: the proposed methodology was applied to the Ecuadorian National Interconnected System (NIS) to assess the impact of an eruption of the Cotopaxi volcano. iii) Resilience metrics: a variety of metrics are described to quantify the resilience of EPS in the context of volcanic hazards in terms of operational and infrastructure performance.

The remainder of this paper is organized as follows. Section II presents the proposed methodological framework to evaluate the ash deposit impact on EPS. Section III presents the case study and results, and Section IV summarizes the main conclusions and future research works.

II. Methodology

The proposed methodological framework is illustrated in Fig. 1 and contains six stages (A-F in the figure) that are detailed below.

A. Ash deposit georeferenced data sampling

In this stage, ash deposit data sampling is carried out by performing simulations using the Ash3d volcanic ash dispersion model of the United States Geological Survey (USGS) [11]. Ash3d uses three-dimensional, time-varying wind fields and other meteorological properties to calculate where airborne ash is transported under current or historical atmospheric conditions. In this way, specifying the volume of the pyroclastic flow erupted in cubic kilometers based on historical volcanic eruption index (VEI) data, KMZ output files of ash deposit patterns can be generated (a KMZ file is a geographic annotation placemark file in latitude and longitude coordinates).

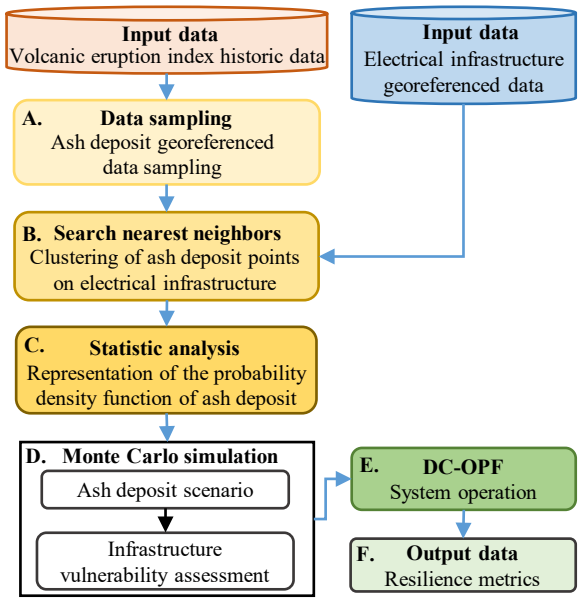

Fig. 1. Proposed methodology to assess the impact of ash deposition on electric power systems.

B. Clustering of ash deposit points on electrical infrastructure

Ash deposit on electrical infrastructure is determined by clustering all ash deposition points with the georeferenced power system components. All ash deposition points are obtained from KMZ files described in Stage A. The following components are included in this study: generators, substations and transmission line insulators. It should be noted that line insulator flashover rather than line breakage is considered because transmission lines are historically robust against ash deposit. [12].

Fig. 2(a) presents a clustering example of ash deposit points on the power system components. C_1 and C_2 represent the georeferenced electrical components (generators, substations or transmission line insulators). The clustering process considers the distance between the ash points (grey x) obtained from the KMZ files and the electrical components (d_1 and d_2). The radius r depends on the resolution of the mesh considered in the Ash3d software. Fig. 2(a) shows no ash deposit points in the radius r for component C_1. On the other hand, for component C_2 there are two ash deposit points within r. Furthermore, because d_1 is less than d_2, the ash deposit value of only the closest point (d_1) is assigned to C_2. In this way, a sample of ash deposition data for each electrical component is obtained to determine the probability density function in the next stage.

C. Representation of the probability density function of ash deposit

Once the ash deposit data has been sampled in each electrical component of the EPS in Stage B, a probability density function is required to perform the MCS in in the next Stage D. Due to the complex sampling process, the generated data might

978-1-6654-0823-3/22/$31.00 ©2022 IEEE

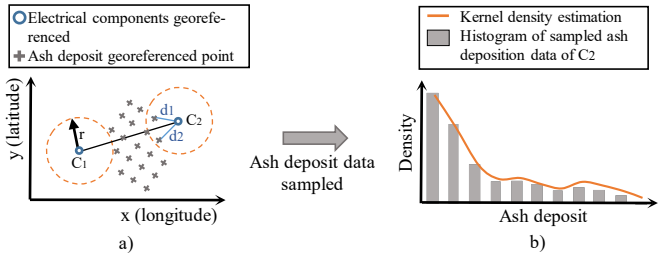

Fig. 2. (a) Representation of the probability density function of ash deposit. and (b) Kernel density estimation.

not be attributed to any well-known distribution function; therefore, non-parametric methods are needed, which can be applied regardless of the proper distribution of the data [13]. In this Stage C, we use a kernel distribution, which is a non-parametric representation of the probability density function of a random variable and is defined using data sampling [14]. Fig. 2(b) presents the kernel density estimate for the ash deposit of C2 compared to the histogram of sampled data and illustrates how kernel density estimation converges to the proper density function for the sampled ash deposit data.

D. Monte Carlo simulation

This stage involves two steps. In the first step, ash deposit scenarios are generated using MCS through the probability density functions obtained in the previous stage to characterize the ash deposit on electrical infrastructure. In the second step, an infrastructure vulnerability assessment is carried out. The damage probability of the generators, substations and transmission line insulators are determined using vulnerability curves. In this work, the vulnerability curves represent the probability of exceeding a given damage state of system components as a function of the ash deposit in millimeters. We use the vulnerability curves presented in [12] illustrated in Fig. 3, which were obtained from the data on ash deposit impacts. Once the damage probability is obtained for the vulnerable components of the EPS, it is assumed that the electrical infrastructure will not be available if the probability of damage is higher than an established probability threshold. Furthermore, we assume that a transmission line will not be available if any of the insulators of that line are unavailable because of flashovers due to ash accumulation. In this way, the unavailability matrices by contingency scenario of buses $(A_{n,s})$, power plants $(A_{i,s})$ and transmission lines $(A_{l,s})$ are determined by MCS using the software MATLAB R2019a [15].

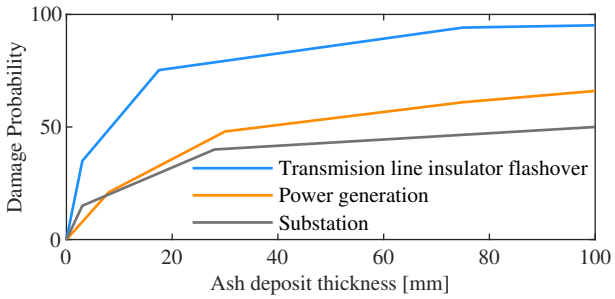

Fig. 3. Vulnerability curves for power generation, substation and transmission line insulator flashover.

E. System operation

The operation of EPS against the occurrence of different contingency scenarios in its electrical components is determined by the resolution of a DC-OPF model. The DC-OPF model considers the resulting impacts of many states of the system, including the intact system state (s=0) and simultaneous outage scenarios. These impacts are usually measured in terms of energy not supplied (ENS) and valued through economic metrics such as the value of lost load (VoLL). The DC-OPF model was implemented and solved using FICO® Xpress [16].

The mathematical formulation of the DC-OPF model corresponds to linear programming defined by equations (1)-(12). This DC-OPF model under contingency was deployed and used in [3].

$$\text{Minimize} \left\{ \sum_{g\in G} \pi_g^{op} \cdot P_{g,s=0} + \sum_{s\in S} \sum_{n\in N} VoLL_n \cdot ENS_{n,s} \right\} \quad (1)$$

subject to:

$$\sum_{g\in G_n} P_{g,s} + \sum_{h\in H_n} P_{h,s} + \sum_{r\in R_n} P_{r,s} + \sum_{l\in L|to(l)=n} f_{l,s} - \sum_{l\in L|fr(l)=n} f_{l,s} + ENS_{n,s} = D_n \cdot A_{n,s} \quad ;\forall n\in N, s\in S \quad (2)$$

$$\sum_{g\in G} R^{up}_{g,s=0} + \sum_{h\in H} R^{up}_{h,s=0} \geq \overline{P_i^{max}} + \gamma \cdot \sum_{n\in N} D_n \;; s{=}0 \in S \quad (3)$$

$$0 \leq ENS_{n,s} \leq D_n \cdot A_{n,s} \quad ;\forall n\in N, s\in S \quad (4)$$

$$0 \leq P_{g,s=0} + R^{up}_{g,s=0} \leq P_g^{max} \quad ;\forall g\in G, s{=}0 \in S \quad (5)$$

$$0 \leq P_{h,s=0} + R^{up}_{h,s=0} \leq P_h^{max} \cdot fp_h \quad ;\forall h\in H, s{=}0 \in S \quad (6)$$

$$0 \leq P_{r,s=0} \leq P_r^{max} \cdot \alpha_r \quad ;\forall r\in R, s{=}0 \in S \quad (7)$$

$$0 \leq P_{g,s} \leq (P_{g,s=0} + R^{up}_{g,s=0}) \cdot A_{g,s} \quad ;\forall g\in G, s\in \{S\backslash s{=}0\} \quad (8)$$

$$0 \leq P_{h,s} \leq (P_{h,s=0} + R^{up}_{h,s=0}) \cdot A_{h,s} \quad ;\forall h\in H, s\in \{S\backslash s{=}0\} \quad (9)$$

$$0 \leq P_{r,s} \leq P_{r,s=0} \cdot A_{r,s} \quad ;\forall r\in R, s\in \{S\backslash s{=}0\} \quad (10)$$

$$-A_{l,s} \cdot F_l^{max} \leq f_{l,s} \leq F_l^{max} \cdot A_{l,s} \quad ;\forall l\in L, s\in \{S\backslash s{=}0\} \quad (11)$$

$$-M(1-A_{l,s}) + \frac{\delta_{fr(l),s} - \delta_{to(l),s}}{x_l} \leq f_{l,s} \leq \frac{\delta_{fr(l),s} - \delta_{to(l),s}}{x_l} + M(1-A_{l,s}) \quad ;\forall l\in L, s\in \{S\backslash s{=}0\} \quad (12)$$

The objective function (1) minimizes the total system operating costs and ENS at a specific period of time (e.g., peak hour). Note that the term VoLL of the objective function represents the cost associated with the value of lost load in each bus. Constraint (2) models Kirchhoff's first law of active power balance between the nodal injections and withdrawals. Constraint (3) models the power reserve margins of the system that must be complied with by conventional generators in the normal operational state to guarantee minimum security levels. Constraint (4) defines the ENS in each node that should not exceed the demand of the node. In addition, constraints (5) and (6) represent the operation limits of conventional power plants (i.e., thermal and hydropower plants). Constraint (7) corresponds to the operation limits of renewable energy plants (e.g., solar and wind) according to the installed capacity and the natural resources available at a specific period of time. On the other hand, constraints (8)-(10) define the operation of the power plants under contingency scenarios, considering the

978-1-6654-0823-3/22/$31.00 ©2022 IEEE

operating conditions and reserve margins determined in the normal state. Constraint (11) represents the transfer capacity limits of the transmission lines operating in contingency status. Finally, constraint (12) models Kirchhoff's second law based on a big-M disjunctive technique [17], where M is a sufficiently large positive constant.

F. Resilience metrics

The performance indicator of expected energy not supplied (EENS) is used to evaluate the resilience of the system. EENS is a standard reliability metric and can be extended for resilience analysis [18]. On the other hand, to measure the performance of specific phases that a power system may experience during an extreme event, the $\Phi\Lambda E\Pi$ resilience metrics can be applied [19]. In this case, the Λ-metric has been chosen to quantify operational and infrastructure resilience degradation after the ash deposition occurs. With this measure, we can compare resilience levels from pre-event levels to the post-event infrastructure and operational resilience levels. The following indicators are used to quantify the Λ-metric:

- The amount of generation capacity (MW) and load demand (MW) that are connected and available for power generation and consumption respectively during the event are used as indicators for the operational resilience.
- The number of transmission lines and buses in service are used as indicators for the infrastructure resilience.

Using the Λ-metric and the indicators described above, the percentage of lost lines, buses, generators and loads are quantified [3].

III. Case Study and Results

The proposed methodology was applied in the Ecuadorian NIS to assess the impact of ash deposits on the power system against an eruption of the Cotopaxi volcano. The Ecuadorian NIS comprises transmission lines at 138 kV, 230 kV, and 500 kV voltage levels. Moreover, it has an installed generation capacity of 7274 MW divided into hydroelectric, thermal, photovoltaic, and wind generation. This generation capacity is sufficient to supply the current peak demand (3953 MW). In addition, there are 63 transmission substations with an installed transformation capacity of 16294 MVA. In addition, it is worth mentioning that the hydroelectric power plants of Ecuadorian NIS are run-of-the-river (operating cost equal to zero), the DC-OPF model implemented only considers the operating cost of thermal power plants in the intact system state. The data required to model the Ecuadorian NIS was obtained from [20] and [21].

In addition, a power reserve margin of the system is established at 10% based on the criteria of reliability and quality of energy service established by the Transmission System Operator (CENACE) [22]. Furthermore, a VoLL is established for the system's substations with a value equal to 1533 USD/MWh. This economic cost is referred to at the national level of the Ecuadorian NIS [23].

We evaluated three case studies according to the erupted pyroclastic flow, based on the most probable VEI of the Cotopaxi volcano (VEI 3-4) [24]. In addition, daily ash deposition simulations were performed with six-year historical meteorological data (from 2015 to 2020). The case studies are detailed below: Case I) Minor case: the erupted volume used is 0.01 km^3, Case II) Moderate case: the erupted volume is 0.15 km^3; and for Case III) Worst case: the erupted volume used is 0.5 km^3. Fig. 4 shows the ash deposition patterns on a random day on the Ecuadorian NIS for the cases described above. These ash deposition patterns evidence that as more erupted volume, the affected area increases.

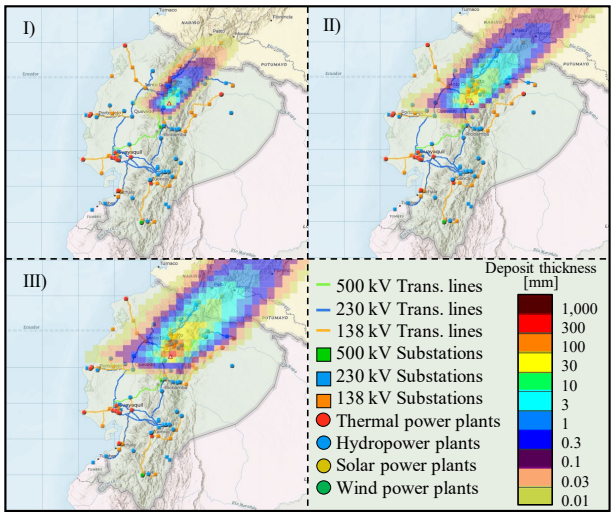

Fig. 4. Ecuadorian National Interconnected System one-line diagram considering ash deposits.

Table I shows the resilience metrics obtained from three case studies on the Ecuadorian NIS after the eruption of the Cotopaxi volcano. These metrics are divided into three groups, including the EENS of the ENS across all scenarios (and economically valued at the VoLL), the operational resilience measured in lost generation and lost load; and the infrastructure resilience measured in outaged lines and outaged buses.

TABLE I
Resilience Metrics Calculated for the Ecuadorian National Interconnected System

		Case I	Case II	Case III
EENS*	**[MWh]**	31	1134	1536
Cost of EENS*	**[MMUSD]**	0.047	1.74	2.35
Operational resilience				
Λ-lost generators*	**[% MW lost]**	0.00	0.27	1.65
Λ-lost load*	**[% MW lost]**	0.00	0.60	1.27
Infrastructure resilience				
Λ-lost lines*	**[% lines outaged]**	2.43	20.00	43.00
Λ-lost buses*	**[% buses outaged]**	0.00	0.40	1.88

* Evaluated through 10000 simulations, ensuring negligible width/error of confidence intervals.

As can be expected, increasing the erupted pyroclastic flow from Case I (minor) to Case III (worst) causes a greater impact in terms of the EENS and the EENS cost, increasing them by 98% from approximately 31 MWh to 1536 MWh and 0.047 MMUSD to 2.35 MMUSD, respectively.

On the other hand, in terms of operational resilience, the metrics indicate that the greater the amount of ash deposited, the percentage of generator and load loss increases progres-

978-1-6654-0823-3/22/$31.00 ©2022 IEEE

sively. These indicators represent a low degradation of the operational resilience of the power system.

Furthermore, in terms of infrastructure resilience, the percentage of lost lines increases considerably as the volume of pyroclastic flow erupted is most critical. Conversely, the percentage of lost buses shows less damage. These indicators demonstrate that the degradation of the infrastructure resilience is more significant due to the accumulation of volcanic ash on insulators, which can lead to flashover. In addition, the evaluation of the resilience metrics can vary according to the geographic location of the EPS in relation to the location of the volcano and volume pyroclastic flow erupted, time-varying wind fields, and other meteorological properties.

The results show that at higher ash deposition such as would be expected in the moderate and worst cases, the impact on the degradation of the power system resilience in terms of energy supply capacity, operation, and infrastructure are more critical. It has to be noted that operational resilience may be lower or higher than infrastructure resilience, depending on the system and on the severity of the event hitting the network. Therefore, the results demonstrate that our proposed methodology is able to assess the impact of ash deposit adequately on EPS.

IV. Conclusions

In this paper, a methodological framework for resilience assessment in EPS against ash deposits after a volcanic eruption is presented. The proposal includes the clustering of ash deposit points on electrical infrastructure to estimate the probability density function. Then, a MCS was performed to determine the unavailability of system elements through vulnerability curves. In addition, a DC-OPF model was included to model the system operation and quantify the operational and infrastructure resilience metrics against the ash deposits. The methodology was applied to the Ecuadorian NIS to use real data in our simulation. The results show that the impact of ash deposit on EPS mainly affects infrastructure resilience due to volcanic ash accumulation on transmission line insulators, causing flashover. Also, it was demonstrated that the methodology can be used to assess resilience in EPS, quantifying the impact on the degradation of the power system resilience in terms of power supply capacity, operation, and infrastructure.

Acknowledgment

The authors would like to thank to "Academic Partner Program" (APP) of FICO® Xpress Optimization Suite. This work has been supported by ANID BECAS/DOCTORADO NACIONAL 21191290, and the Scholarship SENESCYT/ARSEQ-BEC-006295-2018 and SENESCYT/ARSEQ-BEC-006283-2018.

References

[1] Y. Chi, Y. Xu, C. Hu, and S. Feng, "A state-of-the-art literature survey of power distribution system resilience assessment," in *2018 IEEE Power & Energy Society General Meeting (PESGM)*, pp. 1–5, IEEE, 2018.

[2] Y. Wang, C. Chen, J. Wang, and R. Baldick, "Research on resilience of power systems under natural disasters—a review," *IEEE Transactions on Power Systems*, vol. 31, no. 2, pp. 1604–1613, 2015.

[3] M. Saltos-Rodríguez, M. Aguirre-Velasco, A. Velásquez-Lozano, A. Villamarín-Jácome, J. Haro, and D. Ortiz-Villalba, "Resilience assessment in electric power systems against volcanic eruptions: Case on lahars occurrence," in *2021 IEEE Green Technologies Conference (GreenTech)*, pp. 305–311, 2021.

[4] M. Saltos-Rodríguez, M. Aguirre-Velasco, A. Velásquez-Lozano, D. Ortiz-Villalba, and A. Villamarín-Jácome, "Distributed generation for resilience enhancement on power distribution system against lahars occurrence after a volcanic eruption," in *2021 IEEE PES Innovative Smart Grid Technologies Conference - Latin America (ISGT Latin America)*, pp. 1–5, 2021.

[5] A. Velásquez-Lozano, M. Aguirre-Velasco, M. Saltos-Rodríguez, D. Ortiz-Villalba, and A. Villamarín-Jácome, "Optimal planning of var compensator for voltage regulation enhancement on power distribution systems against volcanic eruptions events," in *2021 IEEE Green Technologies Conference (GreenTech)*, pp. 298–304, 2021.

[6] T. M. Wilson, S. Jenkins, and C. Stewart, "Impacts from volcanic ash fall," in *Volcanic Hazards, Risks and Disasters*, pp. 47–86, Elsevier, 2015.

[7] T. M. Wilson, C. Stewart, V. Sword-Daniels, G. S. Leonard, D. M. Johnston, J. W. Cole, J. Wardman, G. Wilson, and S. T. Barnard, "Volcanic ash impacts on critical infrastructure," *Physics and Chemistry of the Earth, Parts A/B/C*, vol. 45, pp. 5–23, 2012.

[8] M. Elissondo, V. Baumann, C. Bonadonna, M. Pistolesi, R. Cioni, A. Bertagnini, S. Biass, J.-C. Herrero, and R. Gonzalez, "Chronology and impact of the 2011 cordón caulle eruption, chile," *Natural Hazards and Earth System Sciences*, vol. 16, no. 3, pp. 675–704, 2016.

[9] J. Wardman, T. Wilson, P. Bodger, J. Cole, and C. Stewart, "Potential impacts from tephra fall to electric power systems: a review and mitigation strategies," *Bulletin of volcanology*, vol. 74, no. 10, pp. 2221–2241, 2012.

[10] G. Wilson, T. Wilson, N. Deligne, and J. Cole, "Volcanic hazard impacts to critical infrastructure: A review," *Journal of Volcanology and Geothermal Research*, vol. 286, pp. 148–182, 2014.

[11] "ASH3D VOLCANIC ASH DISPERSION MODEL available: https://vsc-ash.wr.usgs.gov/ash3d-gui/#!/," June 2021.

[12] A. Wild, T. Wilson, M. Bebbington, J. Cole, and H. Craig, "Probabilistic volcanic impact assessment and cost-benefit analysis on network infrastructure for secondary evacuation of farm livestock: A case study from the dairy industry, taranaki, new zealand," *Journal of Volcanology and Geothermal Research*, vol. 387, p. 106670, 2019.

[13] P. H. Kvam and B. Vidakovic, *Nonparametric statistics with applications to science and engineering*, vol. 653. John Wiley & Sons, 2007.

[14] A. W. Bowman and A. Azzalini, *Applied smoothing techniques for data analysis: the kernel approach with S-Plus illustrations*, vol. 18. OUP Oxford, 1997.

[15] "Matlab avaliable: https://www.mathworks.com/products," Sept. 2020.

[16] "Fico xpress optimization suite avaliable: http://www.fico.com/en/products/," Sept. 2020.

[17] L. Bahiense, G. C. Oliveira, M. Pereira, and S. Granville, "A mixed integer disjunctive model for transmission network expansion," *IEEE Transactions on Power Systems*, vol. 16, no. 3, pp. 560–565, 2001.

[18] M. Mahzarnia, M. P. Moghaddam, P. T. Baboli, and P. Siano, "A review of the measures to enhance power systems resilience," *IEEE Systems Journal*, vol. 14, no. 3, pp. 4059–4070, 2020.

[19] M. Panteli, P. Mancarella, D. N. Trakas, E. Kyriakides, and N. D. Hatziargyriou, "Metrics and quantification of operational and infrastructure resilience in power systems," *IEEE Transactions on Power Systems*, vol. 32, no. 6, pp. 4732–4742, 2017.

[20] "PLAN MAESTRO DE ELECTRICIDAD available: https://www.recursosyenergia.gob.ec/plan-maestro-de-electricidad/," Sept. 2020.

[21] "INFORME ANUAL 2019 available:http://www.cenace.org.ec/index.php?option=com_phocadownload&view=category&id=6:phocatinfanuales&Itemid=50," Sept. 2020.

[22] "PROCEDIMIENTOS DE DESPACHO Y OPERACION (VERSION 2.0) available: https://www.regulacionelectrica.gob.ec/wp-content/uploads/downloads/2015/10/ProcedimientosDespacho.pdf," Sept. 2020.

[23] "INFORME DE SEÑALES REGULATORIAS PARA LA RENTABILIDAD E INVERSIÓN available: https://www.cier.org/es-uy/Lists/Informes/Informe%20CIER%2008_Generacion_%202015.pdf," Sept. 2020.

[24] P. Vera, P. Ortega, E. Casa, J. Santamaría, and X. Hidalgo, "Modelación numérica y mapas de afectación por flujo de lahares primarios en el drenaje sur del volcán cotopaxi," *Revista Politécnica*, vol. 43, no. 1, pp. 61–72, 2019.